Journal of Imaging Science and Technology® 50(1): 17–24, 2006.

Color Management of Four-Primary Digital Light Processing Projectors

David R. Wyble▲ and Mitchell R. Rosen▲
Munsell Color Science Laboratory, Rochester Institute of Technology, 54 Lomb Memorial Drive, Rochester, New York 14623

Abstract. *Traditionally, hardware for additive color displays, including projection devices, has been built from a set of only three primaries: a red, a green, and a blue. Recently, some manufacturers of projector displays have designed their hardware to project a fourth primary, a white. This fourth primary has been helpful in increasing the luminous output possible from these displays. Because interdevice color communication infrastructure is based on red, green, and blue channels (RGB), the four-primary devices accept RGB digits and internally convert to red, green, blue, and white channels (RGBW). From a color management viewpoint, the four-color projectors look like RGB devices, but the typical color characterization models fail owing to the complexity introduced by the hidden RGB to RGBW conversion. Several four-primary digital light processing projectors were investigated and a new characterization model is proposed that approximately accounts for the relationship between RGB digital counts and resultant projected colorimetry. © 2006 Society for Imaging Science and Technology.*
[DOI: 10.2352/J.ImagingSci.Technol.(2006)50:1(17)]

INTRODUCTION

Data projectors are often used in demanding imaging applications requiring accurate color. To properly control the color output of such devices, one needs accurate color control models. A color management algorithm for a four-color projector is proposed. The examined projectors are based on hardware and internal controls developed by Texas Instruments (TI) for their digital micromirror technology[1] known as digital light processing (DLP). The TI four-primary configuration[2] is found in data projectors produced for the office and lecture room market. The digital cinema line of DLP projectors[3] is based on a red, green, and blue channels (RGB) color rendering approach, which is not covered by this article.

Four-channel color displays have relatively recently been introduced to the market. The displays of interest here have the traditional RGB and also a supplemental white channel (W). In parallel to the four-color printer problem, a fourth channel in a display creates a color reproduction challenge since there exist many colors, represented as single points in a three-dimensional color space, that can be mapped to multiple red, green, blue, and white combinations. A further complication of these projectors is that at the computer interface they are treated as RGB displays. That is, projectors are addressable as typical three-channel devices. The conversion from RGB to red, green, blue, and white channels (RGBW) takes place internally making them at once compatible with current RGB display signals and yet unfriendly to simple color management approaches.

The characterization of a display forms the foundation of a mapping from device digital coordinates to colorimetry. This is referred to as the "forward model." A common method for characterizing typical RGB color displays starts with three one-dimensional input look-up tables (LUTs) for linearizing the digital input signals with respect to tristimulus values (*XYZ*). This is followed by a 3×3 matrix for scalar rotation, completing the transformation to tristimulus space.[4] Extending this model to a four-channel display is straightforward: the fourth channel needs its own linearization LUT and the rotation matrix becomes a 3×4 matrix. If the RGBW channels of these projectors were all directly controllable, then this would represent the forward model. Unfortunately, the projector only accepts RGB digital coordinates and internally converts them to RGBW. Thus, the forward model must also account for this conversion.

To complete the color management of a projector, an inverse model is needed to convert from colorimetry back to device digital coordinates. For these displays, such a model needs to solve both the one-to-many problem of *XYZ* to RGBW as well as the transformation from RGBW back to RGB. As is often the case with a complex color rendering device, a reasonable forward model is not always readily inverted.

There are several published efforts regarding the use and characterization of projection displays. Some of these papers have described characterizations of LCD-based projectors.[5,6] Studies have been performed on the details of implementing multiple-projector systems.[7] Much theoretical research has been done on the design and modeling of DLP systems.[1,2,8,9] Wyble and Zhang demonstrated a forward characterization model.[10] Describing the derivation and implementation of an inverse model[11] completes the color management picture for these DLP engines.

FOUR-PRIMARY DLP PROJECTION TECHNOLOGY

The schematic of a representative four-color DLP projector is shown in Fig. 1. A rotating filter wheel sequentially filters the broadband light source. After filtering, the beam is focused onto the digital micromirror device (DMD). The

▲IS&T Member

Received Mar. 24, 2005; accepted for publication Jun. 16, 2005.
1062-3701/2006/50(1)/17/8/$20.00.

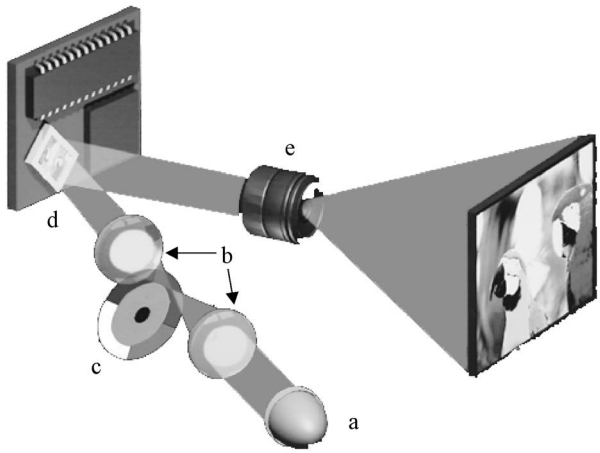

Figure 1. Diagram of four-color DLP projection system: (a) light source; (b) input optics; (c) filter wheel, (d) DMD; and (e) exit optics and screen.

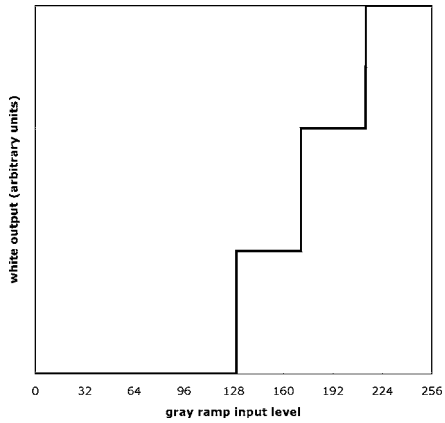

Figure 2. White addition scheme described in Kunzman and Pettitt (after Fig. 6 in Ref. 2).

DMD is an addressable array (e.g., 1024×768) of mirrors which are able to direct incident light in two directions, approximately ±10°. In the course of imaging a frame, a pixel of a given separation (red, green, blue, or white) is selected by directing light incident on a single mirror toward the output optics. Mirrors corresponding to areas of the image not containing that separation direct incident light into a light trap. The mirror positions on the DMD are adjusted on a kilohertz time scale, beyond video frame rates. The perception of full color is due to the temporal integration by the eye and brain of the four channels successively flashed to the screen.

The strategy for white addition has been outlined.[2] The method for determining the quantity of white is based on the input RGB request. White is added in a small number of discrete levels when the requested color approaches or exceeds that which can be produced with RGB separations alone. White is coarsely quantized so the controller trades RGB with W. In a color or gray ramp this transaction means that each time the amount of white is increased, an appropriate amount of RGB is removed to offset the relatively large amount of light that is added with the higher white level. RGB separations can then be increased again until another unit of white is required. This is shown graphically in Fig. 2. Once all of RGB and W are at their respective maximums, the gamut boundary of the device is reached.

The model presented later approximately captures the tradeoffs that are implemented in the device. While it likely falls short of a complete mimicking of the underlying physical properties and algorithmic complexities of the device, the utility, simplicity, and most importantly the low error of the model justifies its use for many applications.

CHARACTERIZATION MEASUREMENTS

An Optoma™ EzPro 755 four-primary projector was used for the majority of the experiments described later. Unless otherwise specified, all references to "projector" will indicate this device. This projector has a 1024×768 pixel DMD, and a stated output of 2000 ANSI lumens. The video signal was generated through the XVGA video output of a standard Macintosh G4 PowerBook computer. The measurement device was an LMT C1210 colorimeter. The C1210 was placed in the center of the field approximately 2 m from the projector. All images were uniform over the entire field, and were displayed for about 5 s prior to measurement, sufficient time for both the projector and measurement device to stabilize at the given setting.

The colorimeter was configured to return *XYZ* tristimulus values for the 1964 10° standard observer. All reported measurements and color calculations were made in this way. CIELAB calculations were normalized relative to the whitepoint of the projector. That is, the CIELAB X_n, Y_n, and Z_n came from the measured *XYZ* at R=G=B=255.

The brightness and contrast controls of the projector were adjusted to eliminate clipping at low or high levels. Clipping will compromise the robustness of an inverted model. If projector settings were desired that imposed clipping, the predictive ability of the model will decrease due the the inability to create appropriate LUTs.

Specific measurements made were the red, green, blue, and equal-digit ramps, as well as a large set of verification data. Ramps were measured every fifth digital count except for the ranges 0–10 and 245–255, where every digital count was measured. The equal-digit ramp is simply R=G=B for the same range of digital counts. (For consistent terminology, use of "white" will be used only for the actual white separation.) The higher sampling in the shadows and highlights allow a probing of projector behavior in these often critical regions. For verification data a 10×10×10 matrix of RGB colors was measured. To avoid any changes that might occur in projector behavior over time, ramp measurements and verification data were taken at each session. Characterization results for this projector were consistent with those of a second DLP-based projector, described later, and with projectors characterized in previous work.[10]

The individual ramp responses were compared to the equal-digit ramp response. Figure 3 shows the *Y* tristimulus value of the equal-digit ramp (black line), and the sum of *Y* tristimulus values of the R, G, and B ramps (dashed line),

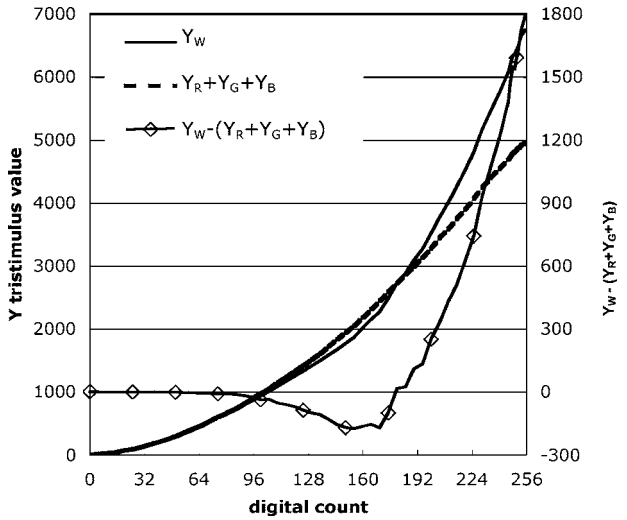

Figure 3. Comparison of equal-digit ramp and sum of responses from R, G, and B ramps. Note secondary ordinate axes for the difference plot. Negative areas of the difference plot show digital counts where the output of the combined RGB ramps exceeds that of the equal-digit ramp for the same digital count.

and their difference (solid line with symbols, note secondary ordinate axis). For a typical additive color device the equal-digit and the sum of the RGB individual curves would be expected to nearly coincide. Under optimal conditions, only system and measurement noise should cause the equal-digit and summed RGB curves to mismatch in a standard RGB device. The fourth channel changes this expectation. The difference between the equal-digit ramp and the summed RGB ramps indicate places where white is mixed into the system. For this projector, all colors produced above a digital count of 175 on the equal-digit ramp indicate white addition.

More curious is the behavior between digital counts of about 60 and 175. Here, the sum of RGB exceeds the equal-digit ramp. This is counterintuitive. Similar behavior has been noted in all DLP projectors characterized to-date: Seven different projectors from various manufacturers. Engineers at Texas Instruments[12] indicated surprise that measurements show less light in this digit range than would have been projected with the sum of RGB channels alone in that range. One possible explanation is that parameters to the TI RGB to RGBW algorithm were based on slightly different projectors, accounting for inaccuracies found in the trade-off assumptions for these projectors. The model presented later is robust to this situation.

THE FORWARD MODEL

The forward model accepts RGB digital input coordinates and predicts the output color *XYZ* produced by the projector. The forward model is identical to one previously reported;[10] this model can be summarized in Eqs. (1) and (2):

$$R' = rLUT(R),$$

$$G' = gLUT(G),$$

$$B' = bLUT(B),$$

$$W' = wLUT\{\min(R,G,B)\}, \tag{1}$$

$$C_{\text{out}} = \boldsymbol{M} C_{\text{in}} \tag{2}$$

where C_{out} is the output color *XYZ*, C_{in} are the linearized scalars, R', G', B', and W'; $\boldsymbol{M}$ is the 3×4 rotation matrix plus a dark correction making it 3×5. $\boldsymbol{M}$ is derived as

$$\boldsymbol{M} = \begin{bmatrix} X_R^c & X_G^c & X_B^c & X_W^c & X_K \\ Y_R^c & Y_G^c & Y_B^c & Y_W^c & Y_K \\ Z_R^c & Z_G^c & Z_B^c & Z_W^c & Z_K \end{bmatrix}, \tag{3}$$

where *X*, *Y*, and *Z* are measured tristimulus values and the subscripts *R*, *G*, *B*, *W*, and *K* are for full red, full green, full blue, calculated white, and black (residual light when R=G=B=0), respectively. "*C*" superscript indicates that dark correction has been applied. For example, the calculation for dark corrected *XYZ* values is shown in Eq. (4) for the red primary. Green and blue corrections take place analogously

$$\begin{bmatrix} X_R \\ Y_R \\ Z_R \end{bmatrix}^C = \begin{bmatrix} X_R - X_K \\ Y_R - Y_K \\ Z_R - Z_K \end{bmatrix}. \tag{4}$$

Equation (5) shows the calculation of the dark corrected white column. It is the difference between the sum of the dark corrected tristimulus values of the full red, green, and blue primaries and the dark corrected equal-digit ramp response

$$\begin{bmatrix} X_W \\ Y_W \\ Z_W \end{bmatrix}^C = \begin{bmatrix} X^c_{255,255,255} - (X_R^c + X_G^c + X_B^c) \\ Y^c_{255,255,255} - (Y_R^c + Y_G^c + Y_B^c) \\ Z^c_{255,255,255} - (Z_R^c + Z_G^c + Z_B^c) \end{bmatrix}. \tag{5}$$

Intuitively, the white *XYZ* values on the left-hand side of Eq. (5) describe the "leftover" color that is outside of the range of the RGB separations for a given input level.

The four channel tone response curves are shown in Fig. 4. They are derived from the measured *XYZ* data. R, G, and B curves are normalized values of the *X*, *Y*, and *Z* values, respectively, of the R, G, and B ramps. The white tone response accounts for the amount of luminance measured from the equal-digit ramps that exceeds the sum of the RGB separations. Therefore, the summed *Y* values of the red, green, and blue ramps were subtracted from the *Y* values of the equal-digit ramp. For purposes of the forward model LUT, the result was clipped at zero to remove negative components and then normalized to create the white LUT as shown in Fig. 4. Each measurement for the RGB and equal-digit ramps includes some amount of random noise. The multiple subtractions to calculate the white tone response curve increases the noise. The final white LUT shown in Fig. 4 was smoothed with a polynomial to preserve a monotonically increasing LUT. The R, G, and B LUTs were similarly

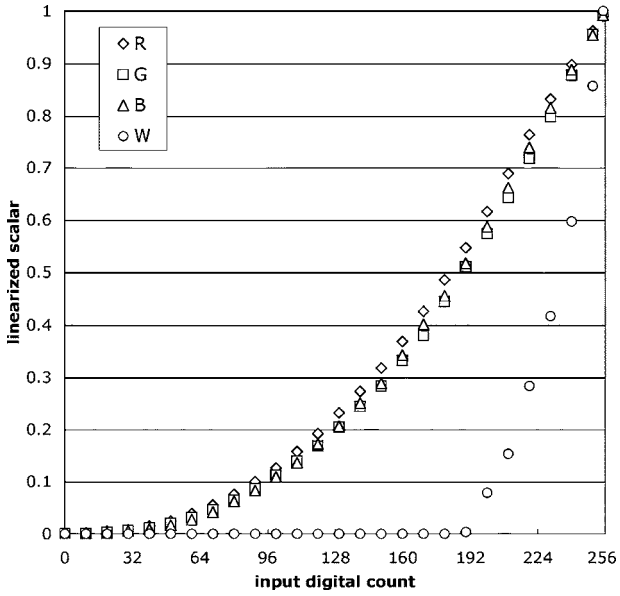

Figure 4. Forward model lookup tables.

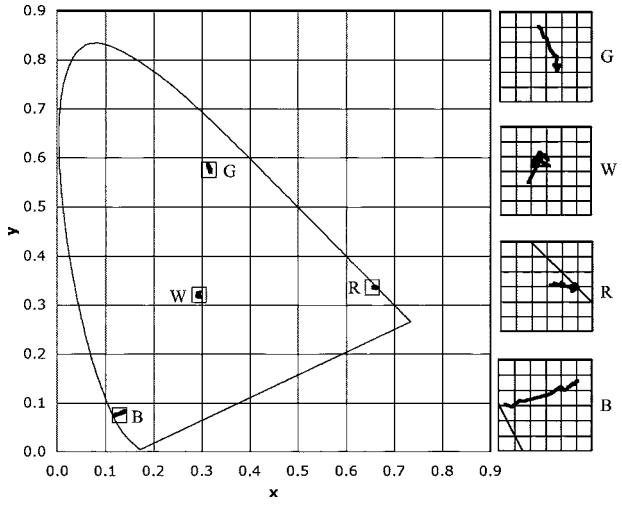

Figure 5. Primary stability. The plot shows *D*65 10° chromaticity coordinates of the R, G, B, and W ramps. Thin solid line is the spectrum locus. Inset plot gridlines are 0.005 units for both axes.

smoothed. As mentioned earlier, adjusting projector brightness and contrast to avoid clipping facilitates the smoothing process significantly. The smoothing also aids in inverting the LUTs, described later, which is required for model inversion.

There are differences between this model and that presented by Kunzman and Pettit.[2] In that work, an outline of the RGB to RGBW internal transformation was presented. Like the currently described model, combinations of only red, green, and blue without any white addition produce all colors within a range of low digits. For both models above certain digits, white is added to all colors. The equal-digit ramp is useful to consider for this discussion. The Kunzman and Pettit description shows a relatively large addition of white at its first introduction (see Fig. 2). Given the large increase of white, a similar decrease in RGB is required to maintain the equal digit response curve. The white level is held steady for many digital counts until a new level of white addition requires another drop in RGB participation.

The current model assumes a continuous addition of small amounts of white to the RGB separations calculated from the individual ramps. Relative to the TI description, there are many places in which the current forward model underpredicts white levels and overpredicts RGB levels. In spite of this probable deviation of the model from actual amounts of RGBW produced by the projector, the LUTs are based on measurements and maintain colorimetric prediction accuracy.

FORWARD MODEL JUSTIFICATION

For the matrix-based forward model to be valid, the tristimulus values of the primaries, represented as columns in the matrix $\boldsymbol{M}$, must not change as the linearized scalars vary across their range. Termed primary stability, the extent to which color devices uphold this requirement can be demonstrated by plotting the chromaticity coordinates of the individual ramp data. These plots are shown in Fig. 5 for R, G, B, and W ramps. The white data in $\boldsymbol{M}$ and Fig. 5 are calculated as in Eq. (5). The inset scales are 0.005 chromaticity units per gridline for both axes of all plots. Note that the subtraction and ratio of very small tristimulus values results in noisy data, and the first few points (corresponding to digital counts of five or less) have been removed from the plot. It can be seen that the primaries vary little, and it will be assumed that this is sufficient justification for the use of the model.

FORWARD MODEL EVALUATION

The forward model was evaluated using the measured verification $10\times10\times10$ matrix of RGB colors. A full factorial of ten levels varied across each separation. Values for each color channel were: 0, 32, 64, 96, 128, 170, 180, 190, 200, 210, 220, 230, 240, and 255. The selection of these values was intended to emphasize the areas of RGB space above 170 digital counts where the projector was potentially adding white. This was to stress the model and ensure that, although the white addition might not be modeled precisely, the model was still accurate for all areas of RGB space.

Figure 6(a), later, is a flow chart showing the data path through the simulation and measurement processes. $\mathcal{F}$ indicates the forward model (transforming RGB to *XYZ*) and $\mathcal{F}^{1}$ indicates the inverse model (transforming *XYZ* to RGB, described later). The assessment of the forward model, shown as "$\mathcal{F}$ verification," is the calculated color difference between the forward model prediction and the measured data for the same RGB coordinates. Figure 7 shows a histogram of the results of the forward model. The mean and maximum color difference for all 1000 points are 1.6 and 3.7 ΔE^{*}_{94}, respectively. Results of the same experiment, but using a different projector (an InFocus LP650, also based on DLP technology) resulted in mean and maximum of 0.5 and 4.2. A similar experiment was run approximately six months earlier using the same Optoma EzPro 755 and an identical

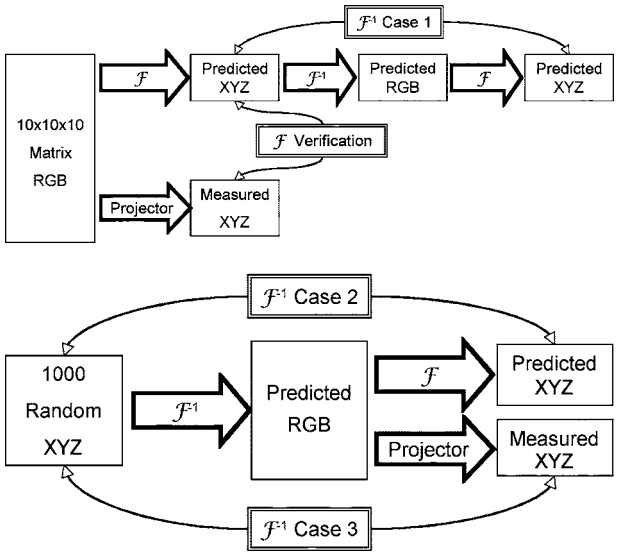

Figure 6. Forward and inverse model data and measurement flow.

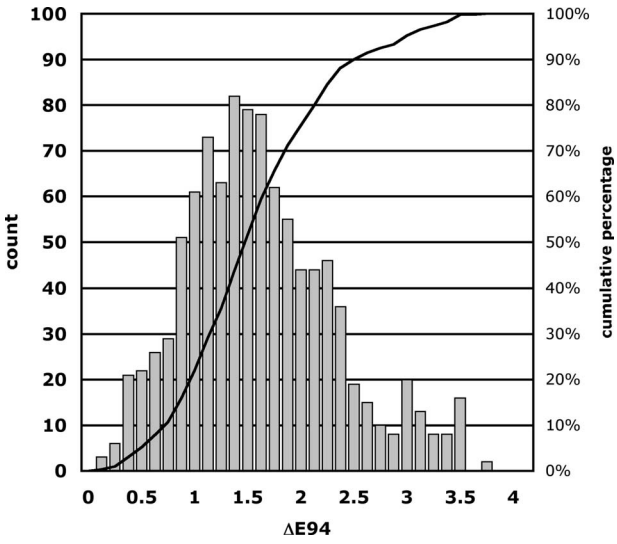

Figure 7. Forward model results. For this and the subsequent histograms, the solid line shows cumulative percentage on the secondary ordinate axes.

measurement setup. The input RGB data set was similarly large, but not identically distributed. The mean and maximum color difference for that test were 1.0 and 3.7, respectively. All of these results are consistent with those previously reported.[10]

THE INVERSE MODEL

When color managing a display as an output device, the inverse model is required. The inverse model accepts a color request, here in tristimulus values *XYZ*, and predicts the input RGB coordinates which, when projected, result in the requested color.

Looking back at Eq. (2), it would be helpful if $\boldsymbol{M}$ could be directly inverted. That would allow linearized RGBW to be easily derived from *XYZ*, solving the inverse problem. $\boldsymbol{M}$ is 3×5 and thus there is no proper inverse. $\boldsymbol{M}$ includes the *K* column that describes the black addition to the predicted color. Performing a black subtraction, as in Eq. (6), reduces the matrix inverse to a 3×4 problem [Eq. (7)], but there is still no proper solution

$$\begin{bmatrix} X \\ Y \\ Z \end{bmatrix}_{\text{request}}^{C} = \begin{bmatrix} X \\ Y \\ Z \end{bmatrix}_{\text{request}} - \begin{bmatrix} X \\ Y \\ Z \end{bmatrix}_{K}, \tag{6}$$

$$\boldsymbol{M}' = \begin{bmatrix} X_R^c & X_G^c & X_B^c & X_W^c \\ Y_R^c & Y_G^c & Y_B^c & Y_W^c \\ Z_R^c & Z_G^c & Z_B^c & Z_W^c \end{bmatrix}. \tag{7}$$

For traditional displays, it is not uncommon to create the transformation matrix from measurements of the individual primaries.[4] $\boldsymbol{M}''$ of Eq. (8) is such a matrix, made from the first three columns of $\boldsymbol{M}$ or $\boldsymbol{M}'$. This matrix is 3×3 and is thus directly invertible

$$\boldsymbol{M}'' = \begin{bmatrix} X_R^c & X_G^c & X_B^c \\ Y_R^c & Y_G^c & Y_B^c \\ Z_R^c & Z_G^c & Z_B^c \end{bmatrix}. \tag{8}$$

The inverse of matrix $\boldsymbol{M}''$ will not be sufficient for predicting the actual RGB′ for much of the gamut. RGB that drive the projector to add white will have dark corrected *XYZ*'s that cannot use the inverse of $\boldsymbol{M}''$ to well predict RGB′. RGB′ for these colors that come from the use of the inverse of $\boldsymbol{M}''$ will be called *theoretical RGB* or RGB_{theo}. See Eq. (9):

$$\begin{bmatrix} R \\ G \\ B \end{bmatrix}_{\text{theo}} = \boldsymbol{M}''^{-1} \begin{bmatrix} X \\ Y \\ Z \end{bmatrix}_{\text{request}}^{C}. \tag{9}$$

For that part of the gamut where no white addition took place, RGB_{theo} is the same as RGB′ and can be pushed through the inverse of the *rgbLUTs* of Eq. (1) to return RGB digital values. As long as all of *R*, *G* and *B* are between 0 and 1, the theoretical RGB should be treated as RGB′.

Should the white addition have been part of the color formation, then at least one of the RGB_{theo} values will be greater than unity. These values can be used to estimate the level of *W*′ in the transform. Recalling from equation (1) that *W*′ is a function of the minimum of RGB, it follows that *W*′ can also be derived from the minimum of RGB_{theo}.

A new set of LUTs, known as LUT_{rgb}^{w} whose derivation is described in the next section are utilized to transform from the minimum of theoretical RGB to *W*′. Once *W*′ is known, the true contribution of white addition can be calculated and subtracted from the requested *XYZ*. This will leave $\boldsymbol{M}''$ as a useful transformation back to actual RGB', solving the inverse function.

Transformation steps are as follows:

(1) Dark correct requested *XYZ* [Eq. (6)].
(2) Calculate theoretical RGB from dark corrected *XYZ* [Eq. (9)].
(3) Check if *R*, *G*, or *B* theoretical is greater than 1. If not, push RGB′ though $rgbLUT^{-1}$ [Eq. (10)]—done.
(4) If *R*, *G*, or *B* theoretical is greater than 1, derive the amount of white addition by pushing *min*(RGB) through LUT_j^w [Eq. (11)] where *j* is *R* if *R* is minimum, *G* if *G* is minimum and *B* if *B* is minimum.
(5) Subtract the white addition from the requested *XYZ* and calculate the RGB′ that would deliver the new *XYZ* [Eq. (12)].
(6) Push the new RGB′ through $rgbLUT^{-1}$ [Eq. (10)]—done.

$$R = rLUT^{-1}(R'),$$

$$G = gLUT^{-1}(G),$$

$$B = bLUT^{-1}(B), \tag{10}$$

$$W' = LUT_j^w \min\left\{\begin{bmatrix} R \\ G \\ B \end{bmatrix}_{\text{theo}}\right\}, \tag{11}$$

$$\begin{bmatrix} R \\ G \\ B \end{bmatrix}' = \boldsymbol{M}''^{-1}\left(\begin{bmatrix} X \\ Y \\ Z \end{bmatrix}_{\text{request}}^{C} - W'\begin{bmatrix} X \\ Y \\ Z \end{bmatrix}_{W}^{C}\right). \tag{12}$$

Determining LUT_j^w

To build the lookup tables used as LUT_j^w in Eq. (11), one needs to find the relationship between the minimum of theoretical RGB values and the associated *W*′. A straightforward approach works well: take RGB combinations, push them through the forward model, first determining *W*′ [Eq. (1)] and then the estimated *XYZ* [Eq. (2)]; then calculate theoretical RGBs from the estimated *XYZ*'s through Eq. (9); finally, make a LUT that relates the minimum of theoretical RGB to determined *W*′.

To make things quite easy, for each separation's LUT, there are only 256 RGB combinations that need be investigated by this method to build that separation's LUT_j^w. The recipe for making LUT_R^w, for example, follows. Do each of the following for R varying from 0 to 255:

(1) Build a RGB triplet from the new *R* value, combined with *G*=*B*=255.
(2) Push RGB through Eq. (1) to RGB*W*′. Maintain the *W*′ value.
(3) Estimate *XYZ* by matrixing RGB*W*′ as in Eq. (2).
(4) Calculate theoretical RGB from estimated *XYZ* [Eqs. (6) and (9)].
(5) Place the $R_{\text{theo}} \Rightarrow W'$ relationship within LUT_R^w.

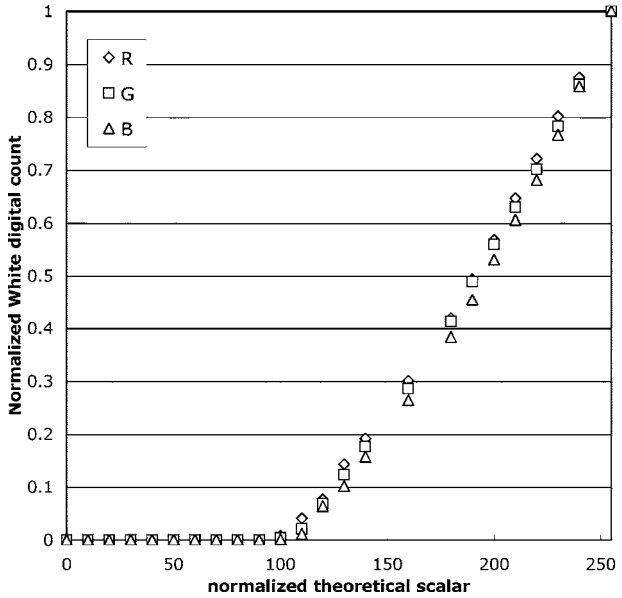

Figure 8. Invert LUTs for determining white addition. In the text, these are referred to as LUT_j^w.

The set of LUT_j^w for this projector are shown in Fig. 8.

For this example the recipe works as long as the $R \Rightarrow W'$ relationship does not change if *G* and *B* in the original RGB change. Recall that the only requirement is that *R* = *min*(RGB). To ensure that this was always true, *G* and *B* were set to 255. Is the $R_{\text{theo}} \Rightarrow W'$ relationship independent of *G* and *B*, so that the same relationship holds even when *G* and/or *B* are not 255?

The answer, as shown in following proof, is yes, the $R_{\text{theo}} \Rightarrow W'$ relationship is independent of *G* and *B*.

Assumption: $R_{\text{theo}} \Rightarrow W'$ relationship is independent of *G* and *B* values where *R* is minimum.

Proof:

Given
red is set to *R*,
green is set to *G*,
blue is set to *B*,
$G \geqslant R \leqslant B$.

By Eq. (1), *R*′ is independent of *G* and *B*; and since *R* = min(RGB), *W*′ is also independent of *G* and *B* by Eq. (1).

Steps 3 and 4 in the earlier recipe use Eqs. (2), (6), and (9) in series. The implicit dark addition step in Eq. (2) is canceled by the dark subtraction step in Eq. (6). Thus the result of steps 3 and 4 could be summarized as the application to RGBW' of the matrix of Eq. (7), M', followed by the inverse of the matrix of Eq. (8), $\boldsymbol{M}''^{-1}$ [see Eq. (13)].

$$\begin{bmatrix} R \\ G \\ B \end{bmatrix}_{\text{theo}} = \boldsymbol{M}''^{-1}\boldsymbol{M}\begin{bmatrix} R \\ G \\ B \\ W \end{bmatrix}'. \tag{13}$$

The inverse of $\boldsymbol{M}''$ could be written as the matrix in Eq. (14):

$$\boldsymbol{M''}^{-1} = \begin{bmatrix} R_{XC} & R_{YC} & R_{ZC} \\ G_{XC} & G_{YC} & G_{ZC} \\ B_{XC} & B_{YC} & B_{ZC} \end{bmatrix}. \tag{14}$$

Due to the well known nature of matrix inverses, the multiplication of Eq. (7) by the inverse of Eq. (8) [as rewritten in Eq. (13)] results in the following:

$$\begin{aligned} \boldsymbol{M''}^{-1}\boldsymbol{M'} &= \begin{bmatrix} R_{XC} & R_{YC} & R_{ZC} \\ G_{XC} & G_{YC} & G_{ZC} \\ B_{XC} & B_{YC} & B_{ZC} \end{bmatrix} \begin{bmatrix} X_R^C & X_G^C & X_B^C & X_W^C \\ Y_R^C & Y_G^C & Y_B^C & Y_W^C \\ Z_R^C & Z_G^C & Z_B^C & Z_W^C \end{bmatrix} \\ &= \begin{bmatrix} 1 & 0 & 0 & (R_{XC}X_W^C + R_{YC}Y_W^C + R_{ZC}Z_W^C) \\ 0 & 1 & 0 & (G_{XC}X_W^C + G_{YC}Y_W^C + G_{ZC}Z_W^C) \\ 0 & 0 & 1 & (B_{XC}X_W^C + B_{YC}Y_W^C + B_{ZC}Z_W^C) \end{bmatrix}. \end{aligned} \tag{15}$$

When substituting Eq. (15) into Eq. (13), it is obvious that theoretical R is dependent only on R' and W'. We have already demonstrated that those two are independent of G and B. Hence, $R_{\text{theo}} \Rightarrow W'$ is independent of G and B. The assumption holds.

INVERSE MODEL EVALUATION

The inverse model was verified in three steps. The data flow and measurement process are diagramed in Figs. 6(a) and 6(b). In this figure, rectangles indicate provided, measured, or calculated data. Arrows indicate processes, either model calculations or projection and measurement. The double-lined rectangles show the comparisons made to evaluate the various steps. The steps each ask questions of increasing difficulty and importance to the usefulness of the model. The simplest question to ask is this: does the inverse model accurately invert the forward model? Shown at the top of Fig. 6(a), "$\mathcal{F}^{-1}$ case 1" is the comparison made to answer this question. Here, initial predicted *XYZ* were the mathematical output of the forward model. Therefore, it was known that this set of *XYZ* precisely corresponded to an input set of RGB. That is, not only were these *XYZ* in gamut, but they corresponded to specific RGB input coordinates which the inverse model should predict from the *XYZ* input.

The second question is similar to the first, but the input set of *XYZ* colors were randomly selected. These *XYZ* were pushed through the inverse model to predict RGB. These RGB are further pushed through the forward model to predict *XYZ*, as shown in Fig. 6(b). For this step each color did not necessarily correspond to a specific RGB triplet. Therefore, quantization error occurred in the rounding of the RGB values predicted by the inverse model. Quantization will potentially induce error in the forward model prediction; the comparison indicated by "$\mathcal{F}^{-1}$ case 2" will show this error in addition to the case 1 error.

The final and most rigorous question asked how well the model performed in a real-world application. Labeled "$\mathcal{F}^{-1}$ case 3," the same set of random *XYZ* values were again pushed through the inverse model; the resulting RGB values were projected; and the projected color was measured and compared to the random input *XYZ* values. In addition to the errors quantified in cases 1 and 2, case 3 exposed errors resulting from measurement and projector variability.

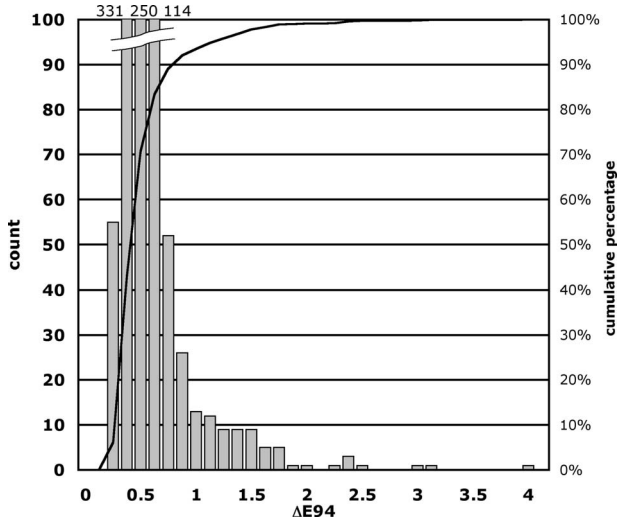

Figure 9. Color difference results for inverse model, step 1.

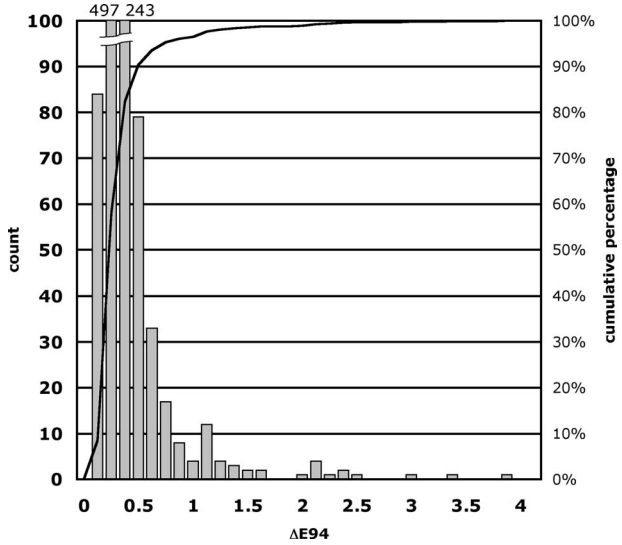

Figure 10. Color difference results for inverse model, step 2.

All three cases were evaluated using ΔE_{94}^*. The whitepoint for the CIELAB calculations was the predicted whitepoint of the projector (R=G=B=255) for cases 1 and 2 and the measured whitepoint for case 3. Histograms of the color difference results are shown in Figs. 9–11 with statistical summaries in Table I.

The results for case 1 are very good, with 90% of the 1000 data points falling at or below 0.5 ΔE_{94}^*. Given that this case was theoretical only, a performance this good should be expected if the inverse model were in fact an accurate inverse of the forward model.

For both cases 2 and 3, the out of gamut colors have been removed from the analysis. Data points were removed

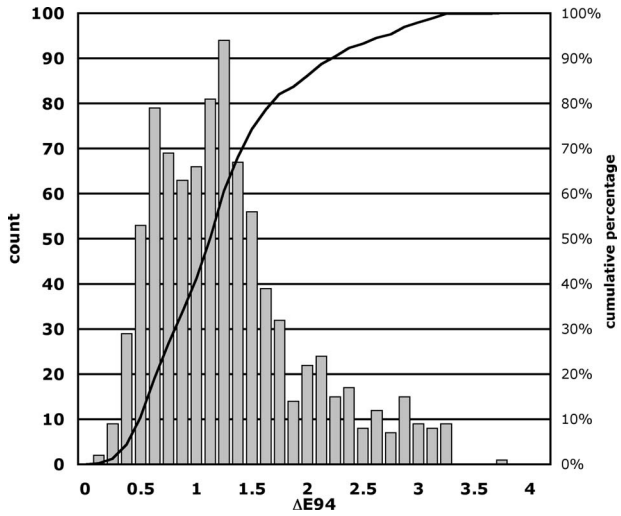

Figure 11. Color difference results for inverse model, step 3.

if their calculated RGB′ [Eq. (12)] were outside the range [0,1]. Case 2 results are nearly as good as case 1, with 90% of the data falling at or below 0.75 ΔE^*_{94}. This case is also theoretical, and these results are not unexpected. The additional error over case 1 is mostly cause by the quantization discussed earlier. Case 3 results show greater color difference; to capture 90% of the data one needs to include color differences up to ΔE^*_{94} of 2.25. Still, this is a very respectable performance for an end-to-end color managed system.

DISCUSSION

A four-primary projector treated as a three-color device but which internally converts RGBs to RGBWs introduces complexity in characterization and inversion for use in color management. The research described here has evaluated four-color DLP projectors and built a model that captures the color characteristics. Inversion of this model required extra lookup tables and steps not usually encountered in evaluating displays. The results show that for many color applications the model offers sufficient accuracy.

Although the projectors have been treated as black boxes for the purposes of this research, earlier disclosures by Texas Instruments indicate that the model described here is not an exact replication of the actual algorithms used within the device to convert from RGB⇒RGBW. This has not hampered the accuracy of predictions. This is because of the vast amount of swapping that can take place between white and RGB. At a certain point in the calculations, the wrong amount of RGB vs W is likely derived. But this interim step does not impact the quality of the colorimetric estimations or, conversely, the choice of RGB digits to match requested colorimetry.

The model assumes that the amount of white projected is only a factor of the minimum RGB value. Given this assumption, an inverse model was demonstrated. A recipe for building the inverse model was given.

Table I. Colorimetric testing results.

Test	Mean ΔE^*_{94}	Max ΔE^*_{94}
Forward model	1.6	3.7
Inverse case 1	0.3	3.8
Inverse case 2	0.5	3.9
Inverse case 3	1.6	3.7
Forward model (2/04)	1.0	3.7
Forward model (InFocus LP650)	0.5	4.2

CONCLUSION

A working forward and inverse color management models have been presented for four-primary data projectors based on DLP technology. The inversion of a previously reported forward model has been shown to work well. The inverse model demonstrates that complete color control can be accomplished accurately enough for many applications. The inverse model is not difficult to derive, and requires no additional measurements over the forward model.

ACKNOWLEDGMENT

This work was supported by the Munsell Color Science Laboratory.

REFERENCES

[1] L. Hornbeck, "Deformable-mirror spatial light modulators", Proc. SPIE **1150**, 86 (1989).
[2] A. Kunzman and G. Pettitt, "White enhancement for color sequential DLP", *SID Digest* **29**, 121 (1998).
[3] G. Pettitt and B. Walker, "DLP Cinema™ technology: Color management and signal processing", *Proc. IS&T/SID Ninth Color Imaging Conference* (IS&T, Springfield, VA, 2001) p. 348.
[4] R. Berns, *Billmeyer and Saltzman's Principles of Color Technology*, 3rd ed. (Wiley-Interscience, New York, 2000).
[5] Y. Kwak and L. MacDonald, "Accurate prediction of colours on liquid crystal displays", *Proc. IS&T/SID Ninth Color Imaging Conference* (IS&T, Springfield, VA, 2001) p. 355.
[6] L. Seime and J. Y. Hardeberg, "Characterisation of LCD and DLP projection displays", *Proc. IS&T/SID Tenth Color Imaging Conference* (IS&T, Springfield, VA, 2002) p. 277.
[7] M. Stone, "Color balancing experimental projection displays", *Proc. IS&T/SID Ninth Color Imaging Conference* (IS&T, Springfield, VA, 2001) p. 342.
[8] S. Lee, C. Kim, Y. Seo, and C. Hong, "Color conversion from RGB to RGB+white while preserving hue and saturation", *Proc. IS&T/SID Tenth Color Imaging Conference* (IS&T, Springfield, VA, 2002) p. 287.
[9] G. Pettitt, A. DeLong, and A. Harriman, "Colormetric-performance analysis for a sequential DLPTM projection system", *SID'96* (1996).
[10] D. R. Wyble and H. Zhang, "Colorimetric characterization model for DLP projectors", *Proc. IS&T/SID Eleventh Color Imaging Conference* (IS&T, Springfield, VA, 2001) p. 346.
[11] D. R. Wyble and M. R. Rosen, "Color management of DLP™ projectors", *Proc. IS&T/SID Twelfth Color Imaging Conference* (IS&T, Springfield, VA, 2004) p. 228.
[12] G. Pettitt (personal communication).